Diffusion in CdS of Cd and S vacancies and Cu, Cd, Cl, S and Te interstitials studied with first-principles computations

2014 Mater. Res. Express 1 025904

(http://iopscience.iop.org/2053-1591/1/2/025904)

Materials Research
Express

Diffusion in CdS of Cd and S vacancies and Cu, Cd, Cl, S and Te interstitials studied with first-principles computations

J L Roehl, Z T Y Liu and S V Khare
Department of Physics and Astronomy, The University of Toledo, Toledo, OH 43606, USA
E-mail: sanjay.khare@utoledo.edu

Received 18 December 2013, revised 14 April 2014
Accepted for publication 23 April 2014
Published 20 May 2014
Materials Research Express **1** (2014) 025904
doi:10.1088/2053-1591/1/2/025904

Abstract
We present an *ab initio* study of the diffusion profiles in CdS of native, Cd and S vacancies, and interstitial adatoms Cd, S, Te, Cu, and Cl. The global minimum and saddle point positions in the bulk unit cell vary for different diffusing species. This results in a significant variation, in the bonding configurations and associated strain energies of different extrema positions along the diffusion paths for various defects. The rate-limiting diffusion barriers range from a low of 0.42 eV for an S interstitial to a high of 2.18 eV for a S vacancy. The rate-limiting barrier is 0.66 eV for Cu and Te interstitials, 0.76 eV for Cl interstitial, 0.87 eV for Cd interstitial and 1.09 eV for the Cd vacancy. The 0.66 eV barrier for a Cu interstitial is in good agreement with experimental values in the range of 0.58–0.96 eV reported in the literature. We report an electronic signature in the projected density of states for the s-and d-states of the Cu interstitial at the saddle point and global minimum energy position. In addition, we have examined the relative charge transfer experienced by the interstitials at the extrema positions through Bader analysis.

Keywords: *ab initio* calculations, cadmium sulfide, diffusion, structural properties, energetic properties

1. Introduction

Cadmium sulfide (CdS) is a large band gap II^B–VI^A semiconductor known for its applications to optoelectronic devices [1, 2]. An important consequence of the large band gap is the high light transmittance of CdS in the visible region. Hence, a prominent use of CdS is found as a window layer for thin film cadmium telluride (CdTe) and copper indium gallium (di)selenide based solar cells. The recent advances in CdTe/CdS thin film technology and fabrication

techniques have allowed CdTe/CdS solar cells to emerge as a leader in the growing market of thin film module production. A number of difficulties have slowed the further improvement of CdTe/CdS thin film technologies. These include the accumulation of Cu, from the back contacts, at the CdTe/CdS interface as well as intrinsic and exotic interstitials originating in CdS and diffusing interstitials from CdTe that cross the interface into the CdS layer affecting the cell performance. The diffusion of Cu into, and its accumulation at, the CdS layer has been the most suspected cause inhibiting long term device stability [3]. All CdS/CdTe cells are exposed to processing temperatures of at least 350 °C during $CdCl_2$ treatment and a chemical reaction between CdTe and CdS can occur, which is the driving force for bulk and grain-boundary inter-diffusion of CdTe and CdS [4]. Diffusion of Cd and Te atoms from the CdTe absorption region into CdS can reduce the light transmission capability of the window in the wavelength region of 500–650 nm. The faster process of diffusion of Cd and S atoms into CdTe, in the opposite direction, is more difficult to control, especially for cell structures with ultrathin CdS films [4]. The effect of Cl in CdS is also well known. Secondary ion mass spectrometry measurements suggest that the high Cl concentration in CdS films yields better solar cell efficiency [5]. Thus, it is well known that semiconductor properties, and hence overall cell efficiencies, are affected by the presence of defects in these layers [6, 7]. To be able to control the defect concentration and mobility of defects in CdS requires understanding of their migration pathways by diffusion in CdS and the structural and electronic properties of these defects. Revealing these bulk diffusion pathways directly is challenging by current experimental techniques alone. These results can be of benefit for the understanding of CdTe/CdS technology by providing the detailed information required for a complete description of diffusion processes that is either difficult to obtain or completely unobtainable experimentally. Experimental investigations of diffusion can provide insight for identification of the diffusion mechanism. However, depending on the technique used, these studies frequently require some treatment of the material or impurity to conduct the experiment. In addition, since 'pure' material samples are an idealization, experimental techniques must also account for the effect of structural defects that are always present in real materials. The experimental work by Borkovska *et al* [8] on diffusion of group I impurity ions in CdS has provided a great deal of information into the anisotropy observed in diffusion both perpendicular and parallel to the *c*-axis. The study concluded that the observed anisotropy is most likely due to the interaction of impurity centers with existing material defects. It is therefore advantageous to investigate the diffusion process from a theoretical bottom-up approach where these extraneous effects can be eliminated and the diffusion processes can be investigated independently. Theoretical investigation not only provides results for values of the energetic barriers for diffusion of defects but also gives insights into the physical mechanism of adatom of vacancy migration and electronic bonding characteristics [9–12]. In addition, recent theoretical work has provided a wealth of information regarding the doping of CdS including the formation energies and ionization levels of native and non-native defects in wurtzite [13] and zinc-blende CdS [14] which considered a range of relevant charge states. However, the computational resources required for examining diffusion mechanisms and the difficulty of the work prohibits such a panoptic study. Therefore, we present results to fill this gap in the literature by investigating the diffusion of neutral charge state defects of Cd, Cu, Te, S and Cl in CdS in this manuscript by *ab initio* computational methods. Further work on many different charge states is relevant and should be undertaken. Our results, from this work, serve as predictions to stimulate further experimental work and supply complementary information about diffusion mechanisms due to the dearth of appropriate experimental techniques.

2. Computational method

We present the results of *ab initio* total energy calculations within the local density approximation (LDA) to density-functional theory [15, 16] for diffusion energy barrier computations using Vienna *ab initio* simulation package [17–20]. Core electrons are treated by ultrasoft Vanderbilt type pseudo-potentials [21] as supplied by Kresse *et al* [22] using the Ceperley and Alder exchange-correlation functional. The single-particle wave functions were expanded in the plane-wave basis using a 200 eV energy cutoff. A gamma centered $2\times2\times2$ k-point grid was used for the Brillouin-zone integrations in all supercell calculations. Tests using larger k-point sampling and higher plane-wave energy cutoff indicated that a numerical convergence better than ±10 meV was achieved. The CdS bulk structure consists of a four atom primitive cell wurtzite structure (space group $P6_3mc$ number 186) with lattice vectors $\vec{a}_1=(a/2)$ $[1, -\sqrt{3}, 0]$, $\vec{a}_2=(a/2)$ $[1, \sqrt{3}, 0]$, $\vec{a}_3=$ a$[0, 0, c/a]$. Both Cd and S atoms occupy 2(*b*) Wyckoff positions (1/3, 2/3, *z*) and (2/3, 1/3, *z*+1/2) where $z=0$ for Cd and $z=$ the internal parameter for S. The lattice constants were varied and fit to parabolic equations as a function of total energy to obtain the absolute minimum in total energy. Using the LDA, the calculated lattice parameters *a* and *c* were 4.09 Å and 6.65 Å respectively, with internal parameter $z=0.376$, are within 1% of the experimental lattice parameters [23] of 4.1365 Å and 6.7160 Å and $z=0.3770$. The calculations were repeated using the generalized gradient approximation (GGA) and the calculated lattice parameters of *a* and *c* equal to 4.23 Å and 6.85 Å respectively, with internal parameter $z=0.376$, were greater than 2% of the experimental lattice parameters. Since the LDA lattice parameters more closely resemble the experimental lattice parameters and energy differences from the true ground state due to motion of the ions are very well represented by either LDA or GGA calculations [24], we have employed the LDA method throughout this work. These computed values give a CdS bond length of 2.50 Å. Diffusion barrier calculations were computed in a 128 atom supercell, a $4\times4\times2$ repetition of the four atom unit cell. The larger supercell size more closely models an isolated defect by reducing the long-range interactions between defects in neighboring supercells. To find the minimum energy for each configuration, all atoms were allowed to fully relax. Relaxation was completed when a force tolerance of 0.01 eV $Å^{-1}$ was reached for each atom. The calculations for the projected density of states (PDOS) were performed with the tetrahedron method with Blöchl corrections [25]. Diffusion barrier calculations were performed using the nudged elastic band (NEB) method [26]. To investigate the quantity of charge transfer of interstitial atoms in equilibrium positions, we implemented a charge division scheme proposed by Bader [27, 28], using the codes developed by Arnaldsson *et al* [29–31]. PAW-LDA potentials were used to include core charges for analysis. We used a $250\times250\times250$ FFT grid to give reliable charge transfer results. Tests with higher grid density for a supercell of the same size indicated that convergence for charge transfer, in units of electronic charge, within ±0.02 was reached.

3. Results and discussion

3.1. Interstitial diffusion

We consider here the diffusion of Cd, Cl, S, Te and Cu interstitials and vacancies of Cd and S. Detailed structural information provided here can only be obtained from reliable DFT

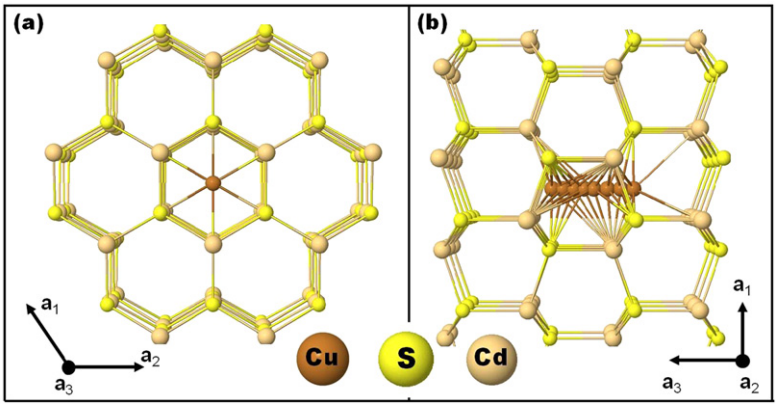

Figure 1. Interstitial diffusion in bulk CdS down the *c*-axis as seen for a Cu adatom (a) parallel and (b) perpendicular to the *c*-axis with several positions of the diffusing Cu interstitial shown. The lattice vectors for the hexagonal wurtzite unit cell are $\vec{a}_1 = (a/2)$ $[1, -\sqrt{3}, 0]$, $\vec{a}_2 = (a/2)$ $[1, \sqrt{3}, 0]$, $\vec{a}_3 = a[0, 0, c/a]$.

computations. It is complementary to results of experimental observations where activation energies are measured indirectly leading to deduction of diffusion barriers [32–42]. The interstitial diffusion paths considered in this work were chosen parallel to *c*-axis. While other interstitial diffusion paths exist, the path parallel to the *c*-axis was chosen as it represents the path that is typically encountered by native and non-native defects diffusing from the CdTe layer because of the lattice matching between zinc-blende CdTe and hexagonal wurtzite CdS, the (0 0 0 1) plane of CdS is often found oriented parallel to the (1 1 1) plane of CdTe [43]. An example of this linear diffusion is shown in figure 1. In the figure, two views of the interstitial diffusion down the *c*-axis are shown. The first one is parallel to the *c*-axis and shows that the entire diffusion pathway occurs symmetrically through the center of hexagons formed by the bulk Cd and S atoms. In the second view several positions of the Cu atoms in various NEB images perpendicular to the *c*-axis are shown. Different species of interstitial adatoms were found to occupy different extrema positions. A single global minimum energy (GME) and saddle point position is found for all the diffusing species considered here. This contrasts with the case of Cu, Ag, Au, Mo, S, P and Sb in CdTe where secondary minima and maxima are found [12]. The GME and saddle point positions for all interstitials are given in table 1. All positions are given in direct coordinates of the wurtzite unit cell. Of these the GME and saddle point positions of Cd, Cl, S and Te show similarities across atomic species in the bonding configuration to neighboring atoms. On the other hand the Cu interstitial behaves differently. We can see from table 1 that the Cd, Cl, S and Te GME occurs between $z = 0.17$ and $z = 0.28$, and the GME for Cu occurs at $z = 0.37$. Similarly, the saddle point for Cd, Cl, S and Te occurs between $z = 0.43$ and $z = 0.55$, and the saddle point for Cu occurs at $z = 0.61$. To investigate the differences between extrema positions in more detail, we focus on the Cd and Cu interstitials.

3.2. Structural properties

3.2.1. Cd. In figure 2, we can see the difference between the Cd and Cu extrema positions. The average bond length and bond angle from the interstitial defects, shown in figure 2, to nearest-neighbors are given in table 2. The Cd interstitial GME position, panel (a), forms a

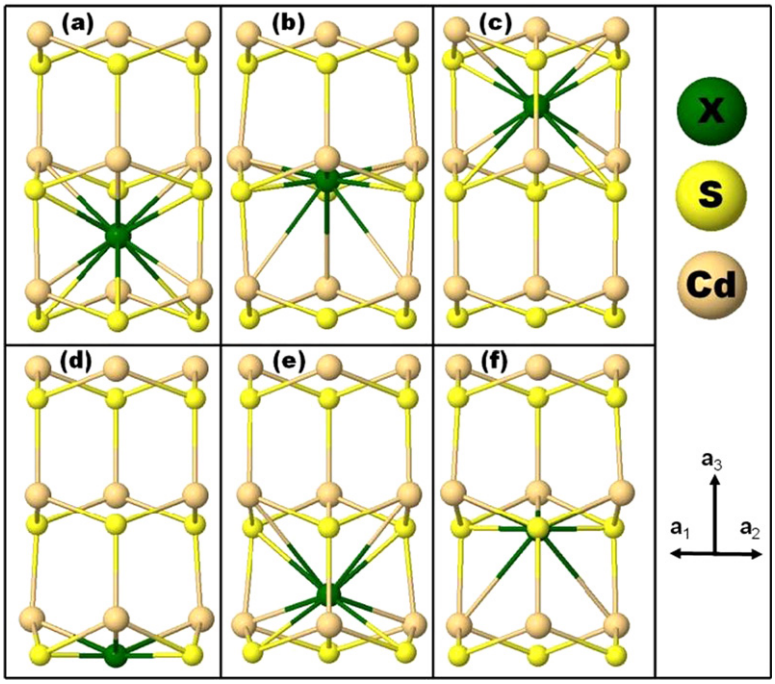

Figure 2. Structural motifs and bonding configuration of interstitial positions along the *c*-axis of minimum and maximum energy. The atom labeled x is the diffusing interstitial atom, the surrounding atoms are of S and Cd. The Cd interstitial begins at the minimum energy position, shown in (a), then diffuses down the *c*-axis until it reaches the maximum energy position, shown in (b), and proceeds until it reaches a another minimum energy position in a neighboring unit cell (c). The same sequence of diffusion steps is shown for a Cu interstitial in (d)–(f). Atoms of S, Te and Cl diffuse similar to Cd.

Table 1. Extrema positions for the diffusing adatoms given in direct coordinates of the hexagonal wurtzite unit cell as, $\vec{R} = c_1\vec{a}_1 + c_2\vec{a}_2 + c_3\vec{a}_3$. For example the S global maximum position is given by $\vec{R}\{S\} = 0\vec{a}_1 + 0\vec{a}_2 + 0.53\vec{a}_3$. Considering the lattice vectors $\vec{a}_1$, $\vec{a}_2$ and $\vec{a}_3$, the c_3 position listed corresponds to the z coordinate.

	Global min			Global max		
Element	c_1	c_2	c_3	c_1	c_2	c_3
Cu	0.00	0.00	0.37	0.00	0.00	0.61
	0.00	0.00	0.87			
Cd	0.00	0.00	0.20	0.00	0.00	0.43
	0.00	0.00	0.70			
S	0.00	0.00	0.25	0.00	0.00	0.53
	0.00	0.00	0.75			
Te	0.00	0.00	0.28	0.00	0.00	0.55
	0.00	0.00	0.78			
Cl	0.00	0.00	0.17	0.00	0.00	0.44
	0.00	0.00	0.67			

Table 2. Average bond length and angle from interstitial defect to nearest-neighbor. The Cd interstitial maximum energy position and Cu interstitial minimum energy position each form a sp^2 like configuration with their respective Cd and S neighboring bulk atoms. The Cd interstitial minimum energy position and Cu interstitial maximum energy position form a distorted octahedral configuration with their respective nearest neighbor bulk S and Cd atoms. For such data the averages of bond lengths and angles are listed along with their ranges in brackets. For example, the Cu interstitial at the global minimum forms a distorted octahedral bonding configuration with six neighboring S atoms. Three S atoms at 2.87 Å making an angle of 87.1° and the other three S atoms at 2.74 Å making an angle of 92.9° for an average bond length of 2.81 Å and an average bond angle of 90.0°.

Element	Position	Figure 1	Nearest-neighbor	Average bond length (Å)	Average bond angle (°)
Cd	Global min	a	S	3.03 (2.77–3.29)	90.6 (78.4–102.8)
			Cd	2.97 (2.83–3.10)	90.2 (83.8–96.5)
	Global max	b	S	2.61	118.5
			Cd	2.69	116.3
Cu	Global min	d	S	2.29	120.0
			Cd	2.72	107.5
	Global max	e	S	2.81 (2.74–2.87)	90.0 (87.1–92.9)
			Cd	3.12 (2.67–3.57)	91.7 (71.4–111.9)

distorted sp^3d^2 like octahedral configuration with the nearest neighbor bulk S atoms with an average bond length of 3.03 Å and angle of 90.6°. Due to the distortion of the octahedral configuration, the Cd interstitial forms a bond length and bond angle of 3.29 Å and 78.4° with three of the S bulk atoms and 2.77 Å and 102.8° with the other three S bulk atoms. Additionally, the Cd interstitial at the GME position forms a less distorted octahedral configuration with the nearest neighbor bulk Cd atoms with an average bond length and angle of 2.97 Å and 90.2°. The distortion of the Cd bulk atoms is less than that of the S bulk atoms with a bond length and bond angle of 3.10 Å and 83.8° with three of the Cd bulk atoms and 2.83 Å and 96.5° with the other three Cd bulk atoms. The Cd interstitial saddle point position, panel (b), forms an sp^2 like configuration with, both Cd and S, neighboring bulk atoms. The bonding with the bulk S atoms is slightly more sp^2 like than the bonding with the bulk Cd atoms. This is indicated by the average bond angle of 118.5° with the three neighboring S bulk atoms, closer to the ideal sp^2 bond angle of 120.0° than the average bond angle of 116.3° the Cd interstitial makes with the three Cd bulk atoms.

3.2.2. Cu. Unlike the Cd interstitial, the Cu interstitial, figure 2(d), forms an sp^2 like configuration with both Cd and S neighboring bulk atoms at the GME position. The Cu interstitial forms an sp^2 bond with the three neighboring bulk S atoms with an ideal bond angle of 120.0° and a distorted sp^2 like configuration with the Cd neighboring bulk atoms. The distortion of the sp^2 like bonds is due to the Cu interstitial being slightly displaced perpendicular to the plane of the Cd bulk atoms resulting in an average bond angle of 107.5°, less than the ideal bond angle of 120.0°. The Cu interstitial saddle point position forms a sp^3d^2 like octahedral configuration with the nearest neighbor bulk S atoms with an average bond

Table 3. Diffusion barriers (eV) for different point defects.

Element	Maximum (eV)
Cu	0.66 (0.58[a], 0.72[b], 0.77[c], 0.96[d])
Cd	0.87
CdV	1.09
S	0.42
SV	2.18
Te	0.66
Cl	0.76

[a] Experimental values from [35].
[b] Experimental values from [32].
[c] Experimental values from [34].
[d] Experimental values from [33].

length and angle of 2.805 Å and 90.0°. The slight distortion of the octahedral configuration creates a Cu interstitial bond length and bond angle of 2.87 Å and 87.1° with three of the S bulk atoms and 2.74 Å and 92.9° with the other three S bulk atoms. The Cu interstitial at the saddle point position also forms a distorted octahedral configuration with the nearest neighbor bulk Cd atoms with an average bond length and angle of 3.12 Å and 91.7°. The distortion of the Cd bulk atoms is less than that of the S bulk atoms with a bond length and bond angle of 2.67 Å and 111.9° with three of the Cd bulk atoms and 3.57 Å and 71.4° with the other three Cd bulk atoms.

3.3. Diffusion barrier and strain energy

From these GME and saddle point positions we have calculated the energetic barriers for diffusion along the NEB pathway. The diffusion barriers for interstitials of Cd, Cl, S, Te and Cu are given in table 3 along with the values for Cd and S vacancy diffusion. The Cd and S vacancy diffusion takes place between neighboring bulk positions in the plane perpendicular to the *c*-axis along the $\vec{a}_1 = (a/2)[1, -\sqrt{3}, 0]$ lattice vector direction. Figure 3 shows the energy (eV) along the diffusion path as a function of the NEB step positions. From table 1 and figure 3 we can see that Cd and Cu interstitials encounter their respective saddle point position earlier in the diffusing path than Te, S and Cl interstitials. The S interstitial has the lowest barrier of 0.42 eV while Cd has the highest barrier of 0.87 eV that is twice that for S. The 0.66 eV barrier for a Te interstitial is large and it is possible that the Te substitution formation energy and barrier is lower than that of for an interstitial of Te. This question is deserving of future investigation but beyond the scope of the current paper. The 0.66 eV value for Cu is in good agreement with experiment. The range of experimental values can be attributed to the different techniques used to determine the barriers including capacitive measurements [32, 33], tracer [34] and optical absorption technique [35]. The calculated diffusion barrier for a Cl interstitial of 0.76 eV is large and this should be viewed as an upper bound for what can happen for diffusion in non-ideal crystals with planar defects such as grain boundaries. The calculation of the diffusion barriers for the S interstitial and vacancy, the lowest and highest values reported, were repeated using the GGA method. The value using the GGA method was 10% lower for the

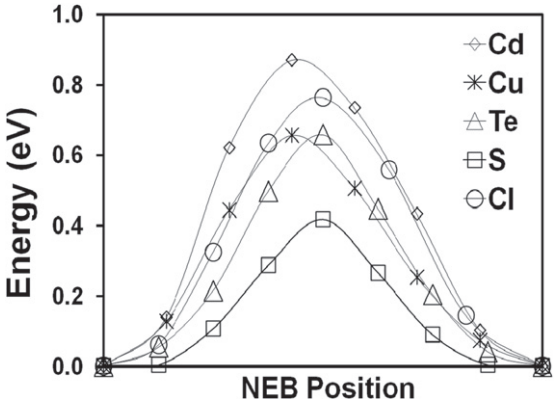

Figure 3. Energy along the diffusion path as a function of the NEB step positions. We observe all interstitial diffusion paths contain a single maximum. For diffusion parallel to the *c*-axis, Cd and Cu interstitials encounter their respective maximum energy position earlier in the diffusing path than Te, S and Cl interstitials. The relative positions of the interstitials at the extrema positions are given in table 1.

largest barrier of the S vacancy, and 25% lower for lowest barrier of the S interstitial, consistent with well-known differences in the two methods [24].

To understand the contribution of strain energy on the total barrier energy we explored the energetics of diffusion by suppressing relaxation of the bulk atoms. To determine the strain energy, an interstitial atom was placed in an un-relaxed bulk cell at the positions determined from the fully converged NEB computations. The energy was computed with the un-relaxed bulk atoms and the interstitial atom fully constrained. From table 1 we can see three distinct minimum energy site (MES) position distributions; one for Cl and Cd with the smallest MES position z coordinates of 0.17 and 0.20, respectively; the second for the next greatest z coordinate S and Te with the MES position $z = 0.25$ and $z = 0.28$, respectively; and the third for Cu with the greatest MES position z coordinates of $z = 0.37$. Figure 4 shows the un-relaxed energy along with the diffusion barrier energy for interstitial atoms of each type, Cd (a), Cu (b) and Te (c). The relaxed energy represents the fully relaxed diffusion barrier energy as a function of the NEB position along the diffusing path. Figure 4 shows that the highest strain energy is not always associated with the saddle point site of the relaxed energy. The highest strain energy for Cd, figure 4(a), does coincide with position of the highest relaxed barrier energy. However, for Cu and Te, figures 4(b) and (c) respectively, the highest strain energy occurs well before the position of maximum relaxed barrier energy. Although Cu and Te share the same diffusion barrier energy of 0.66 eV, we see the wide disparity in strain energy; for Cu the maximum strain energy is around 1.2 eV and for Te the maximum strain energy is almost 5 eV, around four times greater than that of Cu.

3.4. Electronic properties

3.4.1. Charge transfer. In order to further explore the differences between the Cd, Cl, S, Te and Cu interstitials we investigated the electronic properties of the defects in the host CdS. Table 4 shows the electronegativity (χ) [44] and Bader charge transfer (q_{trans}) of the interstitial atoms at their equilibrium positions. We calculated the relative electronegativity with respect to the average electronegativity value of Cd and S, so that $\chi_{\text{CdS}} = (\chi_{\text{Cd}} + \chi_{\text{S}})/2$. Figure 5 shows the

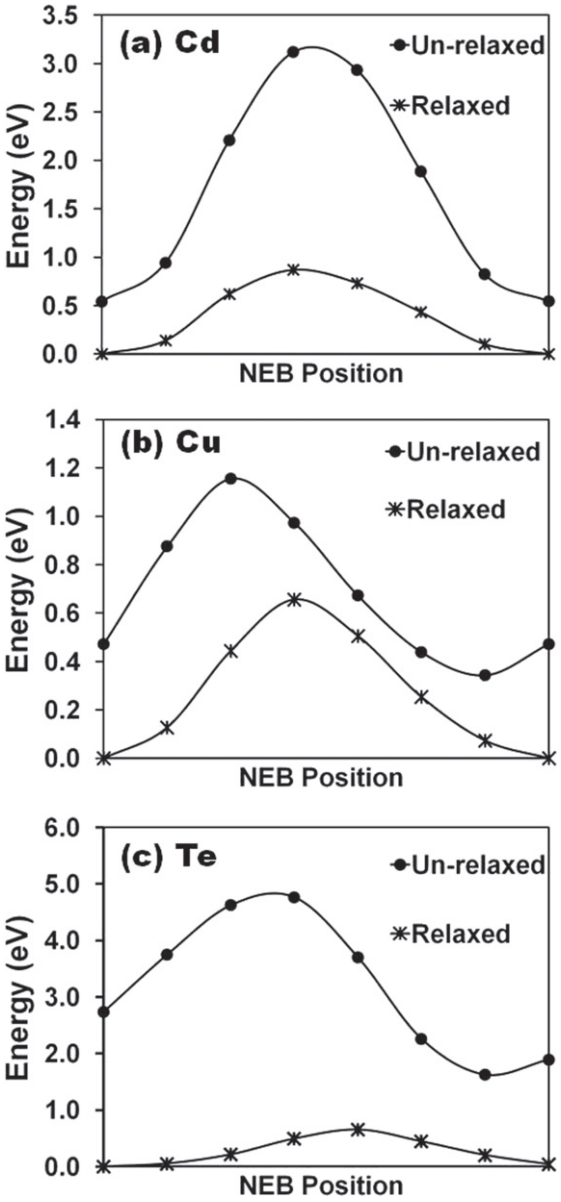

Figure 4. Effect of local strain energy and relaxation around diffusing interstitial atoms of Cd (a), Cu (b) and Te (c). The relaxed energy represents the fully relaxed diffusion barrier energy as a function of the NEB position along the diffusing path; the un-relaxed energy is the energy of the interstitial located at the relaxed NEB position in an un-relaxed bulk cell, i.e. the remaining atoms are left un-relaxed in their bulk positions.

correlation between $\chi-\chi_{CdS}$ and q_{trans}. A monotonic relationship between charge transfer and electronegativity is observed, as expected. We see that Cd and Cu interstitials lose their electrons to the coordinating atoms because their χ is smaller than χ_{CdS}, while S and Cl atoms acquire electrons because they have values of χ larger than χ_{CdS}. The Te interstitial has very minimal charge transfer, and its χ is very close to χ_{CdS}. Since CdS has a composition of 1:1, and the Te interstitial has equal numbers of coordinating Cd and S atoms at similar distances, it is reasonable to expect a minimal charge transfer. We note there is no correlation between the

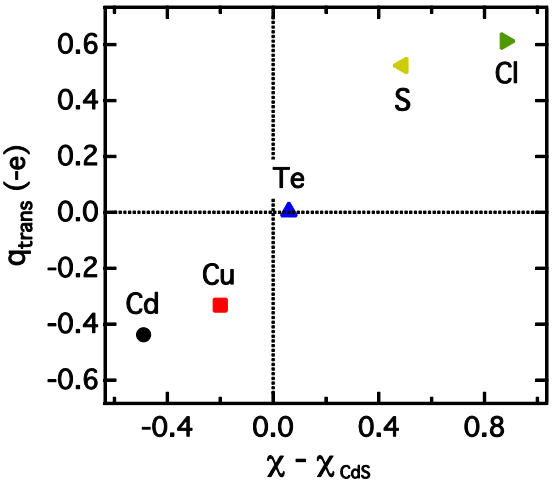

Figure 5. Bader charge transfer (q_{trans}) achieved by the interstitial atoms at their equilibrium position versus its electronegativity relative to its average value of Cd and S (χ–χ_{CdS}). Experimental values of χ are from [44].

Table 4. Electronegativity (χ), relative electronegativity (χ–χ_{CdS}) with respect to the average value of Cd and S (χ_{CdS}) and Bader charge transfer (q_{trans}) achieved by the interstitial atoms at their equilibrium.

Interstitial	χ	χ–χ_{CdS}	q_{trans}(–e)
Cd	1.46[a]	–0.49	–0.44
S	2.44[a]	0.49	0.52
Cu	1.75[a]	–0.20	–0.33
Te	2.01[a]	0.06	0.00
Cl	2.83[a]	0.88	0.61

[a] Experimental values from [44].

stain energy at the MES and saddle point positions and that of the charge transfer. We see that the similar, high values of strain energy possessed by Te and Cd at the saddle point position, compared to that of Cu, are not indicative of the amount of relative charge transfer. The relative charge transfer of Cu is greater than that for Cd but less than that for Te.

3.4.2. PDOS. Since Cu was found to behave differently from interstitials of Cd, Cl, S and Te we analyzed the PDOS for Cu at the MES and saddle point positions. Observation of the metastable transition state or its PDOS is unlikely to be detectable with current experimental techniques. This information presented here, related to the PDOS, obtained using first principles methods is intended to complement experimental work as it provides insight into processes that are otherwise unobservable. Figure 6 shows the PDOS for a Cu interstitial diffusing parallel to the *c*-axis at the minimum and maximum energetic positions. As mentioned, the Cu interstitial forms an energetically favorable sp^2 type bond with the S bulk atoms at the MES position and we note that the bonding of the d-states for Cu correspond primarily to the p-states of the neighboring S bulk atoms. We observe the shift toward deeper binding energies for the d-states of the MES and distinct peak for the s-states of the MES around −6.5 eV that is not present at the saddle point position. At the sp^3d^2 like octahedral saddle point position, the bonds between

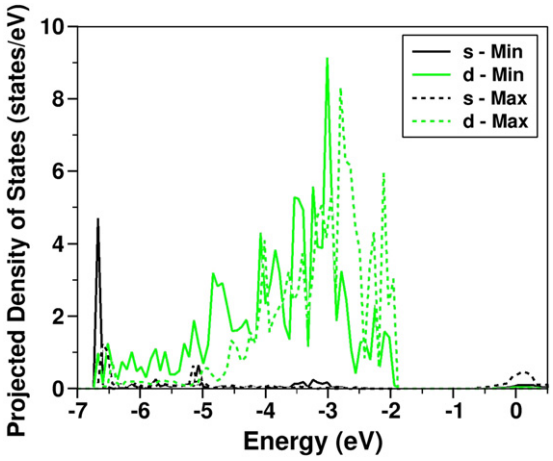

Figure 6. PDOS for a Cu interstitial diffusing parallel to the *c*-axis at the minimum and maximum energetic positions. We observe a shift toward deeper binding energies for the d-states of the minimum. Notable contribution to defect states at the Fermi level from s-states for the maximum position compared to the small contribution from s- and d-states for the minimum is also observed.

the neighboring S bulk atoms and the Cu interstitial have been stretched from 2.29 Å to an average of 2.81 Å and we observe that the d-states of the Cu interstitial are shifted to higher energies closer to toward the Fermi energy. We also note that a sizable contribution to defect states at the Fermi level from s-states for the saddle point position compared to the small contribution from s- and p-states for the GME configuration, is observed.

4. Conclusion

An *ab initio* study of diffusion profiles of native, Cd and S adatom and vacancy, and non-native interstitial adatoms Cu, Te and Cl have been presented here. The rate-limiting diffusion barriers range from a low of 0.42 eV for the diffusion path of an S interstitial to a high of 2.18 eV for the diffusion path of a S vacancy. Differences in structural properties around the diffusing atom or vacancy have been explored for the energetic extrema positions along the diffusion path. The differences were revealed through a description of the first and second nearest neighbor coordination, bond lengths and bond angles. We have examined the amount of charge transfer the defect interstitials acquire at the extrema positions through Bader analysis. In addition, we have found an electronic signature in the PDOS of the s- and d-states for a Cu interstitial at the MES and saddle point positions. These results present predictions for experimental measurements of diffusion barriers and provide other complementary information to experimental findings.

Acknowledgements

The authors would like to thank the Ohio Supercomputer Center (OSC) and the National Science Foundation (NSF), through grant CNS 0855134, for providing computing resources. We thank the Wright Center for PVIC of the State of Ohio and the University of Toledo as well

as the NSF (grants: CMMI 1234777, CMMI 0928440, CMMI 0933069) for funding this work. We appreciate valuable discussions with Prof Alvin D Compaan.

References

[1] Fahrenbruch A L and Bube R H 1983 *Fundamentals of Solar Cells: Photovoltaic Solar Energy Conversion* (New York: Academic Press) pp 418–60
[2] Chopra K L and Das S R 1983 *Thin Film Solar Cells* (New York: Springer)
[3] Dobson K D, Visoly-Fisher I, Hodes G and Cahen D 2000 *Sol. Energy Mater. Sol. Cells* **62** 295–325
[4] McCandless B E and Sites J 2011 *Handbook of Photovoltaic Science and Engineering* 2nd edn ed A Luque and S Hegedus (Hoboken, NJ: Wiley) pp 600–41
[5] Tsuji M, Aramoto T, Ohyama H, Hibino T and Omura K 2000 *J. Cryst. Growth* **214-215** 1142–7
[6] Birkmire R W, McCandless B E and Hegedus S S 1992 *Int. J. Sol. Energy* **12** 145–54
[7] Soo Y L, Huang S, Kao Y H and Compaan A D 1999 *Appl. Phys. Lett.* **74** 218–20
[8] Borkovska L V, Khomenkova L Y, Korsunska N E, Markevich I V and Sheinkman M K 2002 *Phys. Status Solidi b* **229** 269–73
[9] Roehl J L, Aravelli S, Khare S V and Phaneuf R J 2012 *Surf. Sci.* **606** 1303–7
[10] Roehl J L, Kolagatla A, Ganguri V K K, Khare S V and Phaneuf R J 2010 *Phys. Rev.* B **82** 165335
[11] Ma J and Wei S-H 2013 *Phys. Rev. Lett.* **110** 235901
[12] Roehl J L and Khare S V 2014 *Sol. Energy* **101** 245–53
[13] Nishidate K, Sato T, Matsukura Y, Baba M, Hasegawa M and Sasaki T 2006 *Phys. Rev.* B **74** 035210
[14] Wu J-C, Zheng J, Wu P and Xu R 2011 *J. Phys. Chem.* C **115** 5675–82
[15] Hohenberg P and Kohn W 1964 *Phys. Rev.* **136** B864–71
[16] Kohn W and Sham L J 1965 *Phys. Rev.* **140** A1133–8
[17] Kresse G and Hafner J 1993 *Phys. Rev.* B **47** 558–61
[18] Kresse G and Furthmüller J 1996 *Phys. Rev.* B. **54** 11169
[19] Kresse G and Furthmüller J 1996 *Comput. Mater. Sci.* **6** 15–50
[20] Kresse G 1993 *Thesis* Technische Universität Wien
[21] Vanderbilt D 1990 *Phys. Rev.* B **41** 7892–5
[22] Kresse G and Hafner J 1994 *J. Phys.: Condens. Matter.* **6** 8245–57
[23] Sowa H 2005 *Solid State Sciences* **7** 73–8
[24] Kaxiras E 1996 *Comput. Mater. Sci.* **6** 158–72
[25] Blöchl P E 1994 *Phys. Rev.* B **50** 17953–79
[26] Mills G and Jónsson H 1994 *Phys. Rev. Lett.* **72** 1124–7
[27] Bader R F W 1990 *Atoms in Molecules: A Quantum Theory* (New York: Oxford University Press)
[28] Biegler-könig F W, Bader R F W and Tang T-H 1982 *J. Comput. Chem.* **3** 317–28
[29] Henkelman G, Arnaldsson A and Jonsson H 2006 *Comput. Mater. Sci.* **36** 354–60
[30] Sanville E, Kenny S D, Smith R and Henkelman G 2007 *J. Comput. Chem.* **28** 899–908
[31] Tang W, Sanville E and Henkelman G 2009 *J. Phys.: Condens. Matter.* **21** 084204
[32] Lepley B, Nguyen P H, Boutrit C and Ravelet S 1979 *J. Phys. D: Appl. Phys.* **12** 1917–28
[33] Sullivan G A 1969 *Phys. Rev.* **184** 796–805
[34] Clarke R L 1959 *J. Appl. Phys.* **30** 957–60
[35] Szeto W and Somorjai G A 1966 *J. Chem. Phys.* **44** 3490–5
[36] Lane D W, Conibeer G J, Wood D A, Rogers K D, Capper P, Romani S and Hearne S 1999 *J. Cryst. Growth* **197** 743–8
[37] Borsenberger P M and Stevenson D A 1968 *J. Phys. Chem. Solids* **29** 1277–86
[38] Woodbury H H and Hall R B 1967 *Phys. Rev.* **157** 641–55

[39] Jones E D, Malzbender J, Mullins J B and Shaw N 1994 *J. Phys.: Condens. Matter* **6** 7499–504
[40] Jones E D, Stewart N M and Mullin J B 1992 *J. Cryst. Growth* **117** 244–8
[41] Dzhafarov T D, Yesilkaya S S, Yilmaz C N and Caliskan M 2005 *Sol. Energy Mater. Sol. Cells* **85** 371–83
[42] Lyubomirsky I, Rabinal M K and Cahen D 1997 *J. Appl. Phys.* **81** 6684–91
[43] Terheggen M, Heinrich H, Kostorz G, Baetzner D, Romeo A and Tiwari A N 2004 *Interface Sci.* **12** 259–66
[44] Allred A L and Rochow E G 1958 *J. Inorg. Nucl. Chem.* **5** 264–8